Late summer northwestward Amazon plume pathway under the action of the North Brazil Current rings

Léa Olivier, Gilles Reverdin, Jacqueline Boutin, R. Laxenaire, Daniele Iudicone, S. Pesant, Paulo H R Calil, J. Horstmann, Douglas Couet, J.M. Erta, et al.

Remote Sensing of Environment 307 (2024) 114165

Contents lists available at ScienceDirect

Remote Sensing of Environment

journal homepage: www.elsevier.com/locate/rse

Late summer northwestward Amazon plume pathway under the action of the North Brazil Current rings

L. Olivier [a,b,*], G. Reverdin [a], J. Boutin [a], R. Laxenaire [c,d], D. Iudicone [e], S. Pesant [f], Paulo H. R. Calil [g], J. Horstmann [g], D. Couet [h,i], J.M. Erta [j], P. Huber [k], H. Sarmento [k], A. Freire [l], A. Koch-Larrouy [m], J.-L. Vergely [n], P. Rousselot [o], S. Speich [c]

[a] LOCEAN-IPSL, Sorbonne Université-CNRS-IRD-MNHN, Paris, France
[b] Alfred Wegener Institute, Helmholtz Centre for Polar and Marine Research, Bremerhaven, Germany
[c] Laboratoire de Météorologie Dynamique, ENS-Ecole Polytechnique-CNRS-Sorbonne Université, Paris, France
[d] Laboratoire de l'Atmosphère et des Cyclones, LACy, UMR 8105, CNRS, Université de La Réunion, Météo-France, Saint-Denis de La Réunion, France
[e] Stazione Zoologica Anton Dohrn, Villa Comunale, 80121 Naples, Italy
[f] European Molecular Biology Laboratory, European Bioinformatics Institute, Wellcome Genome Campus, Hinxton, Cambridge CB10 1SD, United Kingdom
[g] Helmholtz-Zentrum Hereon, Max-Planck Straße, 1, Geesthacht, 21502, Germany
[h] CNRS, Research Federation for the study of Global Ocean Systems Ecology & Evolution, FR2022 - GOSEE, Paris, France
[i] Station Biologique de Roscoff, UMR7144, ECOMAP, Roscoff, France
[j] EMS, SLU, C/Teodora Lamadrid 40, E-08022 Barcelona, Spain
[k] Universidade Federal de São Carlos (UFSCar), Departamento de Hydrobiologia, Rodovia Washington Luiz S/N., São Carlos, S.P., Brazil
[l] Laboratório de Crustáceos e Plâncton, Departamentode Ecologia e Zoologia, Universidade Federal de Santa Catarina, Florianópolis, Santa Catarina, Brazil
[m] Laboratoire d'Etudes en Géophysique et Océanographie Spatiales (LEGOS), UMR5566, CNES, CNRS, IRD, UPS, Toulouse, France
[n] ACRI-st, Biot, France
[o] IRD, UAR IMAGO, Délégation Régionale Ouest, Technopole Pointe du Diable, CS 10070, 29280 PLOUZANE, France

ARTICLE INFO

Edited by: Menghua Wang

Keywords:
Tropical Atlantic Ocean
Amazon River plume
North Brazil current rings
Ekman transport
Sea surface salinity

ABSTRACT

The North Brazil Current (NBC) flows offshore of the mouth of the Amazon River and seasonally sheds anticyclonic rings (NBC rings) that propagate northwestward and interact with the Amazon River plume (ARP). Mesoscale features have a high temporal variability that is hard to monitor from current weekly and monthly sea surface salinity (SSS) satellite fields. Novel SSS fields with a higher temporal resolution analyzed together with satellite geostrophic currents, chlorophyll-a, and wind speed and in-situ data from the "Microbiomes cruise" on the SV *Tara* in August–September 2021 revealed a late summer freshwater pathway, which was not well documented in earlier studies. By combining these datasets, we improved the characterization of summer ARP pathways. In 2021, the ARP was a succession of freshwater patches cut off from the main plume by the NBC rings. A patch of about 200.000 km^2 with salinity <33.5 pss was observed in September 2021, bringing 0.5 Sv of Amazon water northwestward in a period where the mean ocean currents lead to eastward transport. This patch was shallow, very stratified, and it created a surface steric-height anomaly that was identified as an anticyclonic feature in altimetric sea level products. Once separated from the NBC retroflection, it was mainly driven by Ekman currents. Other similar patches were observed during the 2021 summer, leading to a strong intermittency of the ARP transport. They strongly contributed to make 2021 the year with the largest northwestward freshwater transport in late summer within the 2010–2021 time-period investigated. This freshwater transport pathway is important for all plume-related phenomena, and show the ability of combined SMOS and SMAP data to accurately represent the day-to-day SSS variability.

1. Introduction

The magnitude of discharges from the Amazon River and nearby rivers is unique in the global ocean. It accounts for as much freshwater as the next seven largest rivers in the world combined, contributing to 20% of global river freshwater input to the ocean (Dai and Trenberth, 2002).

* Corresponding author at: LOCEAN-IPSL, Sorbonne Université-CNRS-IRD-MNHN, Paris, France.
E-mail address: lea.olivier@locean.ipsl.fr (L. Olivier).

https://doi.org/10.1016/j.rse.2024.114165
Received 4 August 2023; Received in revised form 14 April 2024; Accepted 18 April 2024
Available online 23 April 2024

The resulting Amazon River plume (ARP) spreads out in the Western Tropical Atlantic (WTA) Ocean over up to 1.3 million of km^2 (Subramaniam et al., 2008), and it brings more freshwater to the northwest tropical Atlantic than the local precipitation minus evaporation budget (Ferry and Reverdin, 2004).

The Amazon discharges at the equator, in-shore of the North Brazil Current (NBC, Fig. 1). The NBC, one of the dominant features of the tropical Atlantic circulation, flows north-westward along the shelves of South America and separates from the shelves around 6–8°N, often to the east of the Demerara Rise. It retroflects seasonally to feed the North Equatorial Counter Current (NECC) and thus closes the equatorial wind-driven gyre. This retroflection occasionally pinches off large anticyclonic eddies called the NBC rings (Johns et al., 1990; Richardson et al., 1994). With a mean radius of 200 km and a diameter that can exceed 450 km, they are the largest rings in the world. The number of rings shed per year varies from 5 (Aroucha et al., 2020; Fratantoni and Glickson, 2002; Goni and Johns, 2001; Mélice and Arnault, 2017) to 9 (Johns et al., 2003). At the surface, the NBC rings strongly interact with the fresh and light waters from the ARP. In particular, near the Demerara Rise (Fig. 1), they have often been associated with plumes of Amazon freshwater separating from the shelf to the open ocean (Olivier et al., 2022; Reverdin et al., 2021).

The river plumes have a significant influence on air-sea exchanges due to their radiative absorption properties and their vertical salinity-driven stratification. They play a role in the formation and maintenance of barrier layers (BL), which trap heat below a shallow surface mixed layer (Saha et al., 2021). Retroactively, the presence of BLs can result in elevating sea surface temperature (SST) by up to 1 °C in the WTA (Foltz and McPhaden, 2009). The BL-induced stratification also suppresses the turbulence induced by the shear, and traps the momentum exchanged between the ocean and the atmosphere in the surface layer (Chaudhuri et al., 2021). Several studies suggest that BLs created by the ARP weaken the mixing induced by tropical cyclones (TC) as well as the entrainment of colder water to the surface, thus contributing to TC intensification (Balaguru et al., 2012, 2020; Ffield, 2007; Grodsky et al., 2012; Reul et al., 2014). The TC season in the Atlantic spans from June to November and peaks in August–September. It is therefore interesting to investigate what controls the advection of the plume's freshwater in the northwestern tropical Atlantic in late summer, a region frequently crossed by TC.

The combined Amazon and Para River discharge usually peaks in May–June (Dai et al., 2009) and is associated with strong northwestward transport of plume water at 5°N, as the NBC retroflection is either weak or nonexistent during this period (Coles et al., 2013). It is followed in August by the largest extension of the plume east of the Lesser Antilles in the northwestern tropical Atlantic, often extending northward of 20°N (Fournier et al., 2015; Salisbury et al., 2011). In August–September however, once the NBC retroflection is established, studies suggest a large dominant feeding of the NECC further east (Coles et al., 2013; Molleri et al., 2010; Muller-Karger et al., 1988).

The NBC rings entrain the fresh and chlorophyll-rich waters originating from the ARP. Using the water color to delineate the rings has led to a better understanding of their generation, evolution and characteristics (Johns et al., 1990; Fratantoni and Glickson, 2002; Ffield, 2005). These analyses suggested that rings can transport Amazon freshwater northwest of the NBC retroflection, which is compatible with Sea Surface Salinity (SSS) maps derived from colored detrital matter associated with the plume (Salisbury et al., 2011; Fournier et al., 2015). Ffield (2007, 2005) reported the presence of Amazon freshwater to the west and north of the NBC retroflection in summer and fall. The author also presented in situ data from other seasons indicating that newly-formed rings are usually surrounded by freshwater or covered by it, and thus that they could contribute to the freshwater transport to the northwest of the retroflection. Saha et al. (2021) found in a MIT general circulation model simulation the presence of Amazon freshwater around the NBC rings in their formation region. Coles et al. (2013) also mentioned the possibility of long-distance transport of freshwater by the rings in their modeling study.

However, the freshwater pathways remain poorly known. Ocean color derived information has often been preferred to satellite salinity to study the ARP and NBC rings because it has a higher temporal and spatial resolution. The rings and the plume are transient features with a strong salinity signature that can move rapidly from day to day. Soil Moisture and Ocean Salinity (SMOS) and Soil Moisture Active Passive (SMAP) missions provides synoptic SSS measurements with a revisit every 2 to 3 days with one satellite, and every day when combining both satellite mission measurements. However, since individual satellite SSS measurements are noisy, the current state of the art level 3 and 4 SSS products are usually averaged over one week or one month (Reul et al., 2020). On the other hand, the ocean color derived information is limited due to the lack of measurements under clouds, and to the imprecision of the relationship between SSS and ocean color, which for instance can be season dependent (Fournier et al., 2015).

In this paper, we revisit the question of freshwater transport to the northwestern tropical Atlantic Ocean during late summer using novel SSS satellite fields with a daily resolution. This product is complemented

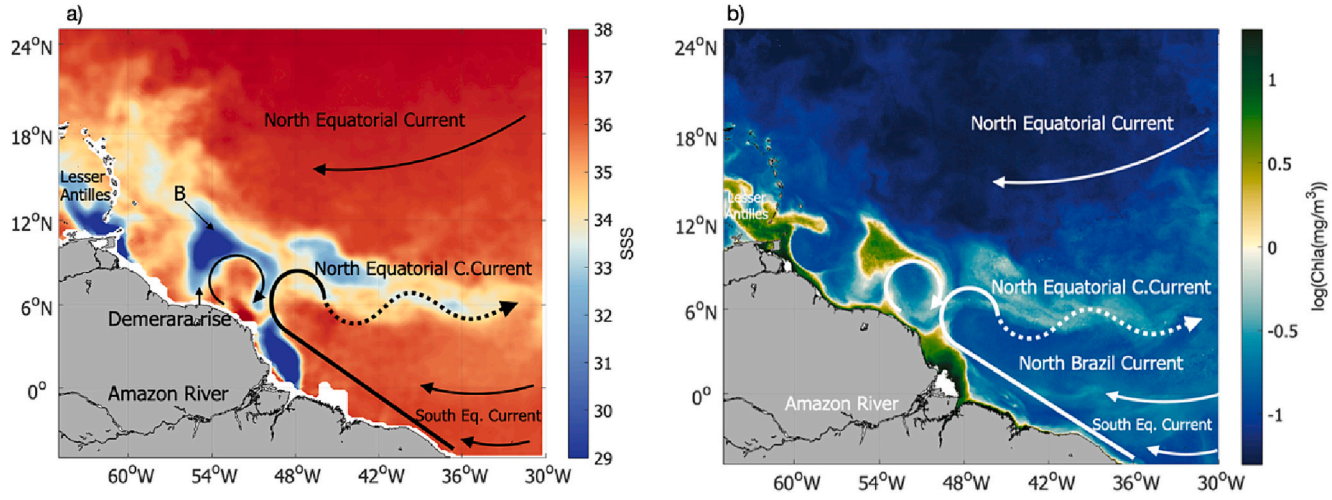

Fig. 1. Main currents and locations superimposed over remote sensing maps of a) sea surface salinity and b) chlorophyll-a on 15 September 2021. SSS and Chla datasets are from Boutin et al., (2022) and Collecte Localisation Satellite (CLS) respectively. On panel a), B refers to the freshwater pool discussed in sections 3.2 and 3.3.

by satellite chlorophyll-a, and geostrophic currents from altimetry as well as data from the 'Microbiomes' cruise on board the sailing vessel (SV) *Tara* in August–September 2021, from drifters and Argo floats. We first investigate the interactions between the ARP and the NBC rings to better understand the mesoscale transport of freshwater in late summer 2021, and the formation of particularly intense freshwater patches. The summer 2021 case study is then extended to other late summers in the period 2010–2021 using satellite observations to track the direction of the freshwater transport.

Data and methods are presented in section 2, before outlining the main results in section 3. We then discuss the results in section 4, and we conclude in section 5.

2. Data & methods

2.1. Ship data

We use salinity and temperature datasets collected by SV *Tara* in August–September 2021, during legs 5, 6 and 7 of the 'Microbiomes' AtlantECO cruise (Fig. 2, Olivier et al., 2023). The 'Microbiomes' project was designed to study the oceanic microbiomes and their interactions with climate and oceanic conditions. In the ARP region, the main aim of the project was to characterize the influence of the ARP and the NBC rings on the biology, biogeochemistry and physics of the region. In this paper we focus on the latter objective. Leg 5 started on 18 August 2021 from Fort-de-France, Martinique and ended in Macapá, Brazil on 9 September 2021. The following Leg 6 from Macapá to Belém (Brazil) started on 12 September until 16 September 2021, whereas leg 7 linked Belém to Salvador da Bahia (Brazil) from 24 September to 8 October 2021. Sea Bird SBE45 and SBE38 instruments continuously measured SST and SSS from water pumped at ~1 m from the sea surface. Although salinity has no unit, we consider the measured salinity variable, or practical salinity, reported on the practical salinity scale (pss) in agreement with international oceanographic commission recommendation on in situ salinity data (IAPSO Working Group on Symbols, 1985). A few long stations (14 to 24 h) with repeated conductivity, temperature and depth (CTD) casts were conducted from SV *Tara* (Fig. 2). The CTD profiles can be used closer to the surface compared to those collected from larger research vessels, as they are free from near-surface mixing induced by the ship's underwater structure at a depth of <2 m. Four to twelve casts were usually repeated in the same site during the 14 to 24 h stations.

A towed instrument array (TIA) from the *Helmholtz-Zentrum Hereon* research center (Kock et al., 2023) was deployed over three sections from SV *Tara* during Leg 5. Ten CTD48M from Sea&Sun Technologies attached to a dyneema rope were deployed while the ship was sailing for a total of 36 h. Depending on the ship's speed, the deepest CTD can reach down to ~55 m. We use the data from two sections across a freshwater patch (Fig. 2). To characterize density stratification, we computed the mixed layer depth (MLD) as the depth of the maximum vertical density gradient. This definition compares well with MLD estimated as the depth with a fixed density change from the sea surface (0.03 $kg.m^{-3}$ for example in de Boyer Montégut et al. (2004)). In the presence of strong near-surface stratification, this definition has the advantage of being less arbitrary on the choice of the uppermost depth in CTD profile retained.

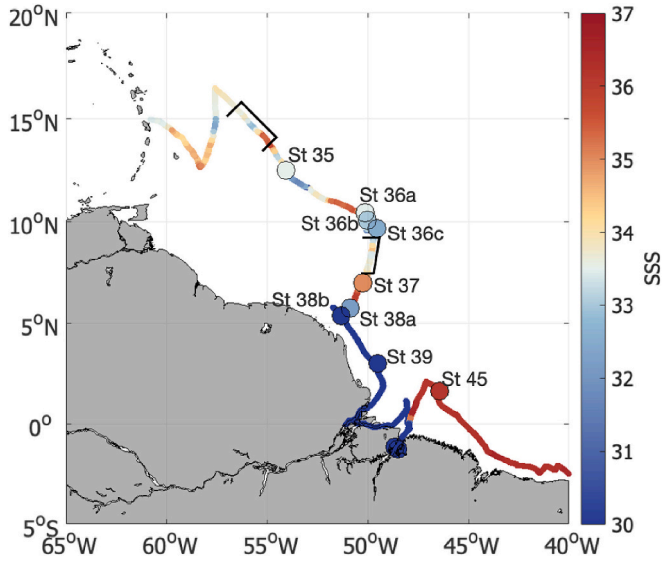

Fig. 2. SV Tara's journey colored by the SSS from the thermosalinograph (TSG). CTD stations are represented by circles, colored by the minimum salinity of the profile. The black frames indicate two sections of the route where the towed instrument array (TIA) was deployed.

2.2. Drifters

We use near-surface currents derived from two types of drifters. Five surface velocity profilers (SVP) drifters drogued at 15-m depth (Lumpkin and Pazos, 2007) were deployed from SV *Tara* and five more from RV *Antea* during the Amazomix cruise (Bertrand et al., 2021) in late August and early September 2021. Given the winds encountered, wind and wave effects on SVP drifters are likely to induce errors smaller than 2 cm/s (Niiler and Paduan, 1995). Additional differences with 15-m currents arise if the drogue is not centered at 15-m depth in sheared surface currents. In addition, 43 small surface followers developed by the *Helmholtz-Zentrum Hereon* research center, referred to as Spot drifters in the following, were deployed from SV *Tara*. They measure the current velocity at 50-cm depth, with a design rather close to the one of CARTHE drifters (Poulain et al., 2022). Here, we focus on the velocities derived south of 12°N and away from the Amazon estuary.

We compared surface velocity in pairs of close-by SVP and Spot drifters (see more details in the supplementary S1). We found differences larger by at least a factor 5 than the expected Stokes drift or other direct wind effect on the small surface float (see Poulain et al., 2022). This most likely results from large near-surface vertical shears in the ARP. The current variability is strong near the NBC retroflection and NBC rings, where merging the surface velocities derived from Spot and SVP drifters will help to better identify patterns of the meso-scale currents.

2.3. Satellite products

2.3.1. Sea surface salinity

Daily SSS maps were initially produced manually following Reverdin et al. (2021) as a blend of the SSS retrieved from the SMOS (Jan. 2010-present) and from the SMAP (Apr. 2015-present) satellite measurements for most days of August and September 2021. Combining measurements acquired from both missions near 6 am and 6 pm local time provides an almost complete coverage of this region with uncertainties on the order of 0.5 pss or less, based on comparisons with ship's TSG SSS (not shown). In this preliminary version of daily SSS maps, we had to manually remove some SMOS tracks strongly influenced by radio-frequency interferences (RFI; Oliva et al., 2016), as well as occasional fresh patches on SMAP maps that were likely due to RFIs. This, together with the actual available tracks, implies a fairly gap-free field was produced only every two to three days. These initial SSS maps are reported in the supplementary material (*Fig. S2*).

To extend this promising but manually built SSS product, the processing chain of the Expertise Center of the Centre Aval de Traitement des Données SMOS (CEC CATDS) has been adapted and applied over 8 regions, aiming at minimizing the temporal smoothing applied to the satellite SSS data. The resulting product was officially called 'CATDS CEC LOCEAN High Resolution SMOS-SMAP SSS maps', and it is the one used in this paper. The product generation and validations conducted

with Argo and TSG in-situ measurements are described in detail on the landing page of the product (https://www.catds.fr/Products/Products-over-Ocean/CEC-Locean-High-Resolution-8-regions) and in the supplementary information (S3). As for the global 18-day CATDS CEC fields (see a general description in Boutin et al., 2018), the high resolution (HR) fields are built using a temporal optimal interpolation (OI), grid node per grid node, and a median over nearest neighbors is applied which leads to a ~ 70 km effective spatial resolution. The temporal OI is done simultaneously with the estimation of SMOS and SMAP SSS systematic errors that depend on the geometry of the satellite acquisition with an approach similar to that described in Boutin et al. (2021). The reduced temporal smoothing of the HR fields results from using an exponential time correlation kernel instead of a gaussian time correlation kernel. The HR fields have been built over the period 2010–2021, combining SMOS and SMAP (after April 2015) data. In the Amazon region, the comparisons to Argo and TSG in situ SSS (Table S3) indicate a reduction of 14% (SMOS only period, 2010–2015) and 29% (SMOS-SMAP period, 2015–2021) of the standard deviation of the differences and the correlation coefficient increased by 5%. The HR fields reproduce well the SSS structures present in the manually made daily product (e.g., supplementary Fig. S2), with a satisfactory removal of most RFI signals.

The HR SSS is compared to the in-situ SSS data from SV *Tara*. The underway *Tara* SSS is measured at 1–1.5 m depth, much closer to the surface than almost all other in-situ data (argo floats, research vessels, ships of opportunity). This is a serious advantage for validating satellite salinity data that are representative of the upper 1-cm of the ocean (Boutin et al., 2016), especially in a region as stratified as the ARP. The validation is detailed in the supplementary materials (S3), and shows that the HR product reproduces well the very low salinities that can be observed in the region. These low salinities are the hardest to capture in averaged weekly to monthly fields, and are key for the study carried out in this paper.

2.3.2. Chlorophyll-a and altimetry derived parameters

Maps chlorophyll-a (Chl*a*) concentration, produced by Collecte Localisation Satellite (CLS) with a spatial resolution of 0.02° and a daily temporal resolution are used. The Chl*a* concentration maps are built from VIIRS (Visible Infrared Imaging Radiometer Suite; on the joint NASA (National Aeronautics and Space Administration)/NOAA (National Oceanic and Atmospheric Administration) Suomi National Polar-orbiting Partnership (NPP) and NOAA-20 platforms) and OLCI (Ocean and Land Color Instrument; on Copernicus Sentinel 3 A and 3B platforms from the European Space Agency) satellite sensors using objective analysis (Pottier et al., 2006). The Polymer software (Steinmetz et al., 2011) is used to compute Chl*a* from the top of atmosphere reflectance. The Chl*a* data is used qualitatively in this study, so the likely contamination by colored dissolved matter and particles in the ARP area is not an issue.

In addition, large scale and low frequency geostrophic currents are used based on daily absolute dynamic topography (ADT) maps distributed by the Copernicus Marine Service (CMEMS) at a ¼° resolution, which combine data from all altimetric satellites available for the period 1993 to present. These delayed-time products typically smooth in time the current structures over typically 10 days, and resolve their variability to 100 km scale. The ADT maps are further used to detect the contours and trajectories of NBC rings using the TOEddies algorithm (Laxenaire et al., 2018). The TOEddies detection algorithm identifies eddies as closed contours of ADT encompassing only one local extremum, and looks for the outermost closed ADT contour around each extremum to define an eddy. It then determines eddy trajectories based on the overlapping of eddy contours at consecutive time steps.

The satellite Chl*a* and SSS maps present mesoscale features in the area of the NBC retroflection and east of the NBC retroflection. For example, a triangular-shaped feature with both very low salinity and high Chl*a* (54°W/10°N), as well as structures associated with an NBC ring to the west of the NBC retroflection are well identified on satellite maps on 15 September 2021 (Fig. 1). The advantage of the Chl*a* product is its high spatial resolution which resolves various filaments and small-scale structures that are smoothed out in the SSS product. In this season, the Chl*a* product covers >95% of the entire region with very little blind areas due to cloud cover.

2.4. Additional datasets

To compute the Ekman transport (see section 2.5.2) and to estimate periods of favored vertical mixing, the wind-stress at a ¼° spatial resolution and daily time steps from the European Centre for Medium-Range Weather Forecasts (ECMWF) Reanalysis v5 (ERA5) is used (Hersbach et al., 2018).

The profiles of Argo floats located inside or in the vicinity of the freshwater patches in September–October 2021 are used to study the MLD (numbers 6900893, 6902838, 6902958, 6902964, 4903352, 4903225, 4903227, 4903226). These floats of types (S2A, Arvor and Provor) have an improved capacity to profile in the presence of strong vertical density gradients as observed in case of low surface salinity compared to earlier floats (Reverdin et al., 2024). Nonetheless, 4 profiles in presence of very fresh surface layers were not successful as the floats could not send the data. Three others only have data up to between 5 and 8 m from the surface, thus not reaching the minimal surface salinity, but still allowing an estimation of the MLD. Altogether, we identified 13 usable Argo float profiles within the most intense fresh patch studied in section 3.2 (not shown).

2.5. Methods

2.5.1. Identification of the freshwater patch

The low salinity mesoscale structure observed in September 2021 is defined as a coherent structure having a salinity below 33.5 pss, i.e., within a closed 33.5 pss salinity contour (Fig. 1). Waters located on the shelf (at a bottom depth shallower than 100 m) are not considered. This threshold allows a good identification of the patch, whereas higher thresholds are not appropriate because a large part of the area east of the Lesser Antilles in late August–October often has salinity between 34 pss and 34.5 pss. Lower thresholds (33 or 32 pss) could have been used but the 33.5 pss threshold allows to track the patch for a longer time (over a full month).

2.5.2. Estimate of the freshwater transport

We estimate the freshwater transport across sections based on satellite SSS, geostrophic and Ekman velocities as follows (similar to Wijffels et al., 1992, but adapted for the ARP region):

$$\frac{1}{\rho_{ref}\cdot S_{ref}}\iint \rho\cdot\left(S_{\mathrm{ref}}-\mathrm{SSS}\right)\cdot \mathrm{V}\cdot \mathrm{dxdz} \tag{1}$$

where ρ_{ref} is the reference density for seawater (1025 kg.m^{-3}), ρ is taken as 1020 kg.m^{-3} to represent the density of the freshwater (average density of water with salinities between 28 pss and 33.5 pss from the TSG), and S_{ref} is the background salinity without the freshwater influence taken as 36 pss. x is the distance along the section, and z is the depth. The velocity is taken as the sum of the Ekman and geostrophic velocity components across the section (for a same layer thickness, and cyclostrophic terms are not considered). The depth of integration is the thickness of the fresh layer.

The Ekman velocity ($\vec{u_{Ek}}$) is computed from the wind stress ($\vec{\tau}$), the depth of the Ekman layer (H_{Ek}), the density ρ, and Coriolis parameter *f* as (Pedlosky, 2012):

$$\vec{u_{Ek}} = \frac{\vec{\tau}}{\rho\cdot H_{Ek}} \wedge \frac{1}{\vec{f}} \tag{2}$$

For consistency, H_{Ek} is taken as the thickness of the fresh layer in (1).

Table 1
statistics of MLD (in m) and of uppermost salinity from the CTD profiles at each station (positions of the CTD stations on Fig. 2).

Station	35	36a	36b	36c	37	38a	38b	39
MLD (mean ± std)	16.2 ± 2.5	13.9 ± 6.5	12.9 ± 1.1	14 ± 6.9	64.1 ± 94.6	3.9 ± 1.4	3.7 ± 1.3	6.2 ± 0.5
S_{min} (mean ± std)	33.4 ± 0.1	33.5 ± 0.1	33 ± 0.07	32.5 ± 0.03	35 ± 0.3	30.7 ± 6.5	25 ± 1.4	29.9 ± 2.5

It is also the same as the mixed layer depth in this region where the stratification is determined by the salinity. It will be estimated in the next section based on in situ data.

3. Results

3.1. Mixed layer depths

The WTA in late summer 2021 is characterized by a large range of mixed layer depths (MLD) ranging between <4 m and >60 m, as indicated by the CTD profiles repeated up to twelve times for each station (Table 1). Time variability of salinity is observed at each site with low salinity (SSS < 34 pss). This variability is particularly strong for stations 38a and 38b in the ARP, with changes of >15 pss within one day (Table 1 and Supplementary Fig. S4). The CTD stations closest to the plume on the shelf indicate MLD shallower than 10 m and fresh layer thickness usually <6 m. Even further north near 10°N (Station 36c) and near 12.5°N (Station 35) the average depth of the fresh layer was only 15 m in surface water with salinity close to or <33.5 pss. The two sections from the TIA towed by SV *Tara* support these observations, and show how MLD covaries with surface salinity and with the fresh layer thickness (Fig. 3). On the first section at latitude 16°N to 13.5°N, the MLD is on the order of 30 m for salinities below 34.5 pss. On the second section, closer to the plume than the first section, the MLD varies from 10 to 20 m, with an averaged MLD of 15 m for salinities below 34.5 pss. Argo profiles located in freshwater patches in September and October support this observation, with a MLD of ~8.5 m in mid-September around 10°N, deepening to ~18 m in late October at 15.5°N (data not shown). Thus, strong haline stratification is observed in surface water with SSS characteristic of the ARP. The MLD thickens as the freshwater plume evolves after separating from the shelf, probably due to lateral and vertical mixing conditions induced by the wind and submesoscale instabilities.

These MLD statistics indicate the presence of a fresh surface layer with MLDs usually shallower than 15 m. This also explains the main differences observed between the Spot and the SVP drifters' velocities: in the ARP south of 7.5°N, the average meridional velocity difference exceeds 32 cm/s. All these instances happen where the fresh water plume is expected to be much shallower than 15 m, enabling large vertical shear between the drogue of the Spot drifter at 50 cm and the drogue of the SVP drifter at 15 m.

3.2. NBC ring and retroflection impact on the ARP and 2021 drifters' trajectories

Near the NBC retroflection and NBC rings, the stratification is not as strong as in the ARP, so we adjusted the Spot drifter velocities to 15-m depth using an estimated downwind shear (Supp Mat. S1, section 2.2) and we got a consistent qualitative agreement with the SVP drifters' velocities at 15-m depth. In these regions, current variability is much larger than in the ARP so that merging the surface velocities derived from Spot and SVP drifters help to better identify patterns of the meso-

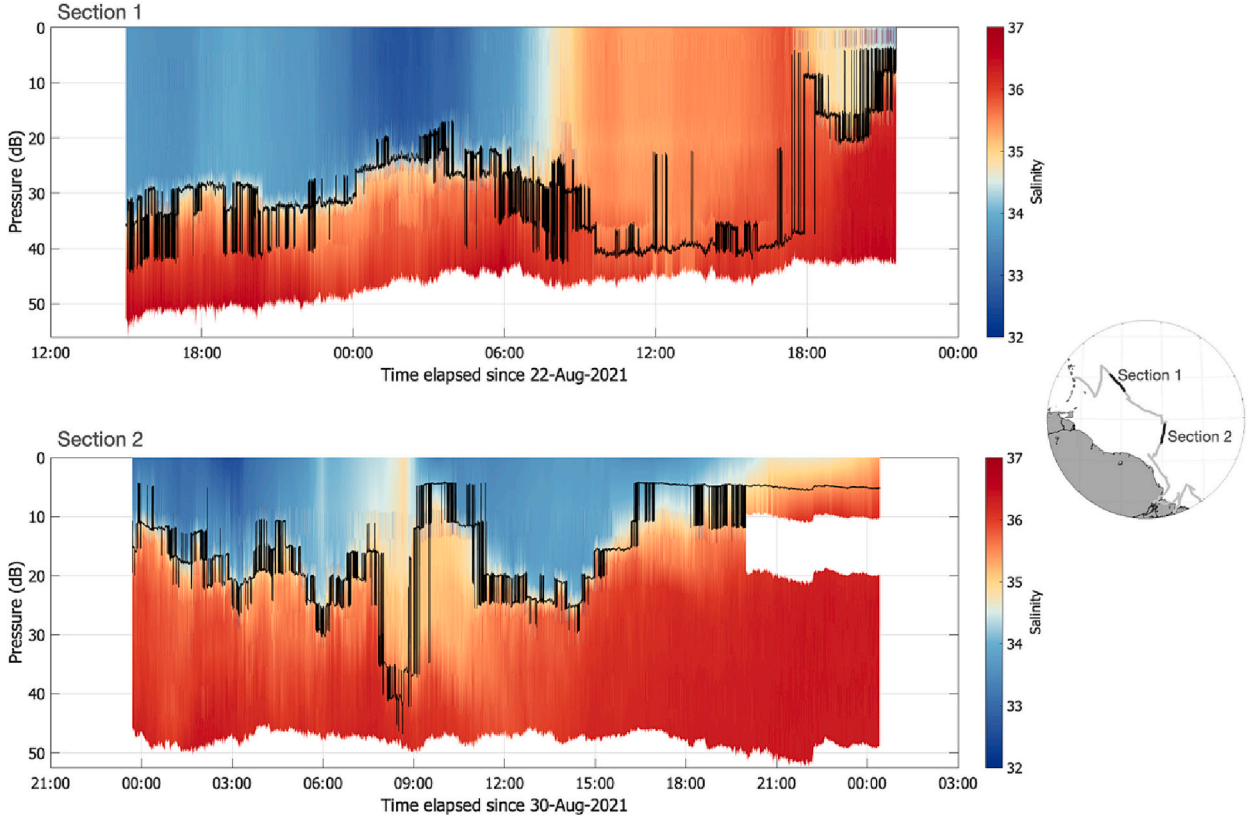

Fig. 3. Salinity along the two TIA sections described on Fig. 2 and on the right panel. During section 1, SV Tara headed towards the south-east, and during section 2, SV Tara headed southward. The mixed layer depth is indicated by the black contour.

scale currents. The largest velocities were observed in the NBC, with velocities faster than 1.8 m/s (SVP, 1.6 m/s for Spot), offshore of the shelf break, reaching up to 5°N (Fig. 4a). The NBC retroflection and NECC showed also velocities of similar magnitude near 7°N, 44°W (Fig. 4b). Beginning of September, several drifters were looping anticyclonically, which points to the surface signature of an NBC ring with a close recirculation. After September 15, the ring was well separated from the NBC retroflection, with many drifters tracking its circulation. The maximum velocities around the ring exceeded 1 m/s (Fig. 4b).

According to satellite salinity maps, the off-shelf ARP coverage increased starting on 1 September 2021 (Fig. 5a). At this date, the NBC retroflection was at its northernmost position around 9°N, as it just formed a well-defined NBC ring based on altimetry-derived geostrophic currents. Initially, the ring was quasi-stationary near the retroflection (*Fig. 5*b). The plume of freshwater rapidly expanded northward, stirred anticyclonically by the NBC ring on 4–8 September, as evidenced by the drifters deployed in the plume (Fig. 4a).

The anticyclonic NBC ring tracked by altimetry and by the drifters' trajectories remained close to the NBC retroflection for more than a month, despite forming a closed recirculation (as detected by altimetry) starting 20 August 2021 (Fig. 5b). The surface core of the ring moved slowly and remained salty (SSS > 35 pss). The ring spent 50% of its lifetime (4.5 months) around 52°W-8°N in the retroflection region until late October, well after its detachment from the NBC around 15 September. Two SVP and 18 Spot drifters circled around the ring, with 4 drifters staying in its core until its demise 100 days later.

As seen on the snapshots of SSS and Chl*a* (Fig. 6), the propagation and evolution of the ARP induced by the ring took place on time scales of days, with velocities diminishing after 8 September (not shown) as the patch of freshwater spreads, leading to its separation from the NBC ring on 12 September. This structure will be referred to as freshwater pool B (Fig. 1). The ring stands out in salinity maps because it entrained fresh water all around it. The freshwater pool B was advected northwestward on 10 September, and circulated around the ring until 20 September (Fig. 6). By 22 September (not shown) and until 1 October, a new tongue of Amazon freshwater extended northward near 50°W to the east of the ring, around a newly reinforced NBC retroflection (*Fig. 6*, panels i and j). One drifter entrained in the retroflection near the slope shows how the plume was connected to the NECC further to the east (*Fig. 4*). However, the northward, then eastward transport of freshwater into the NECC only lasted a few days. By 1 October (*Fig. 6*, panels i and j), the freshwater from the shelf started again to recirculate further west around the NBC ring, as also illustrated by other drifters. This formed another isolated freshwater pool, which moved northward during October (see Section 3.5).

3.3. Drift characteristics and evolution of the freshwater patch

The newly formed freshwater pool B adopted a mushroom-like shape on 8 September (not shown). It evolved until 10–12 September in interaction with the NBC ring, when the ring's proximity to shelf and the Demerara Rise cut off the freshwater supply from the Amazon (Fig. 6 *c,d, e,f*). Part of the eastward side of the patch was still being stretched by the ring circulation until 15 September. This fresh filament shedding resulted in freshwater loss from the patch (Fig. 7). During the months of September and October, there was a northward to northwestward drift of the patch according to the daily satellite snapshots (zonal/meridional displacement velocity on the order of −0.15/0.25 cm.s^{-1}). The structure of the patch became more elongated in early October, with a minimum salinity higher than 30 pss in a core that was still detectable on salinity

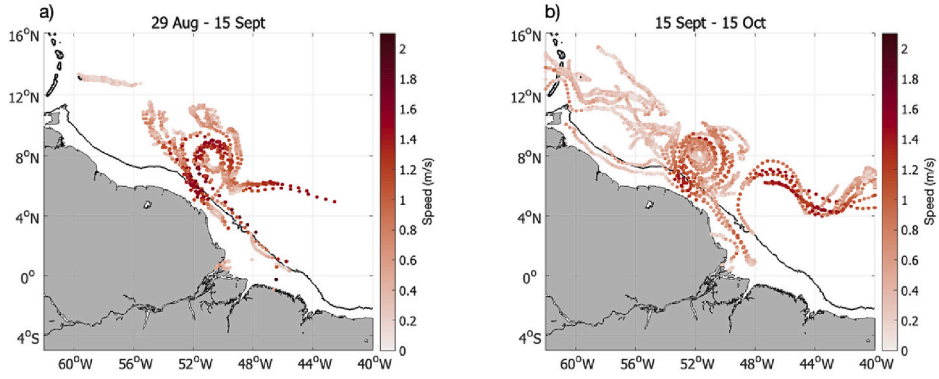

Fig. 4. SVP and Spot drifters' 3-hourly velocity (3 h current) from 29 August to 15 September (a) and from 15 September to 15 October (b). The 100-m bathymetry contour is shown in black. On this figure, the Spot drifters' velocity has been adjusted to 15-m depth by a downwind shear (3.5% of the wind, Supp Mat S1.).

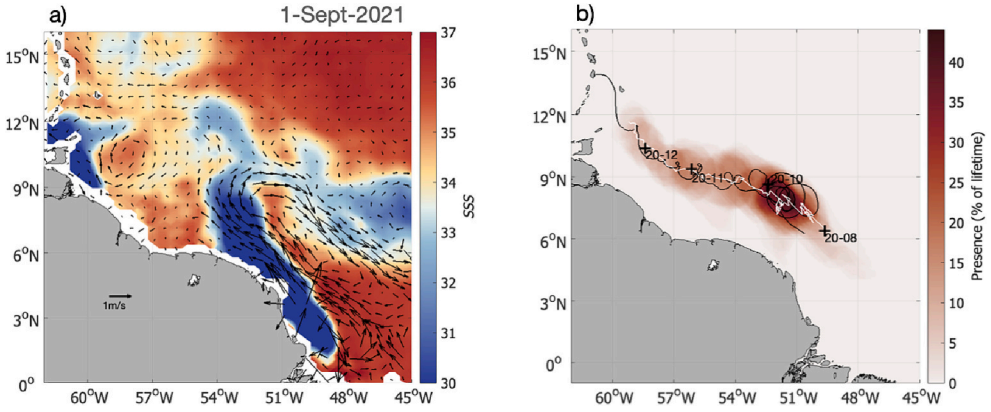

Fig. 5. a) SSS and geostrophic velocities on 1 September 2021. b) NBC ring presence (ratio of time spent in 1 pixel over the full lifetime of the eddy), its trajectory as detected by TOEddies algorithm (white line) and trajectory of Spot drifter 34 trapped in the ring (black line).

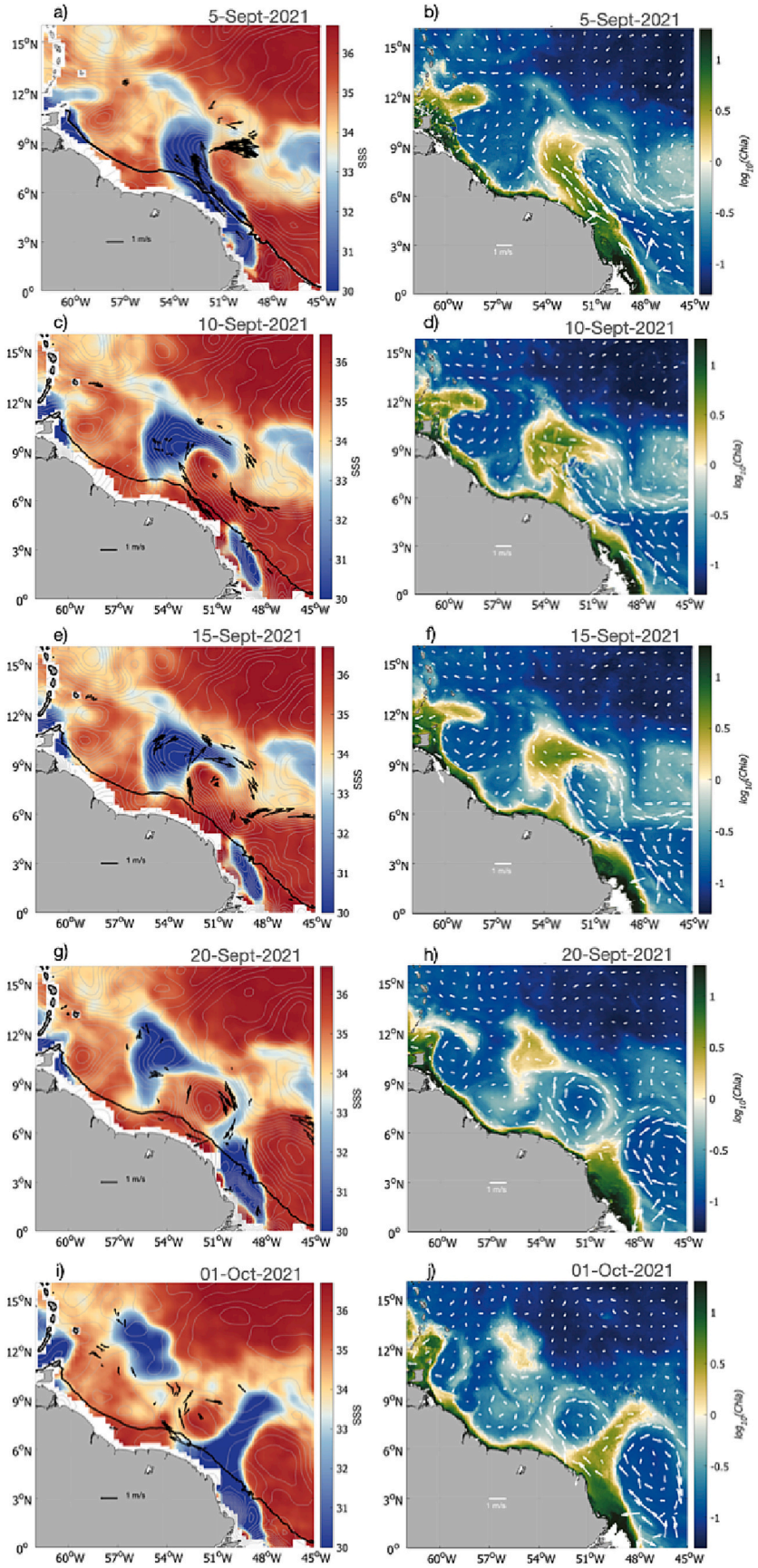

Fig. 6. Snapshots of SSS (left) and Chla (right) following the evolution of the fresh patch over the month of September 2021. The black arrows on top of the SSS represent the drifters' velocities while the white arrows on top of the Chla delineate the altimetric geostrophic currents. The black line on the left panels indicates the 100 m-depth bathymetry.

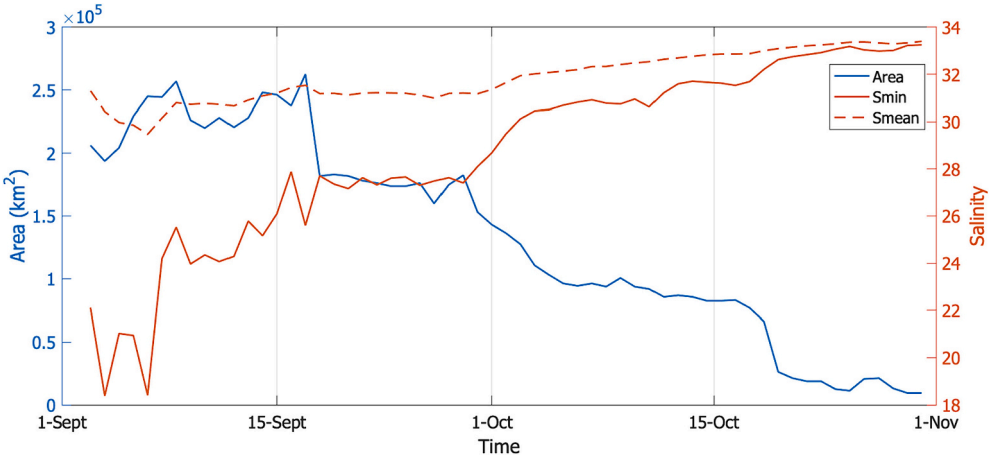

Fig. 7. Area, minimum, and mean salinity of the freshwater pool B defined by a 33.5 pss salinity contour on SSS maps, from 1 September to 1 November 2021.

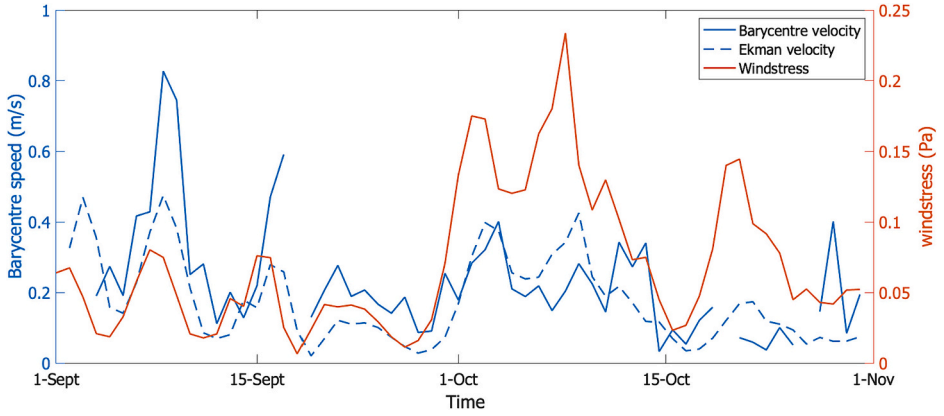

Fig. 8. Velocity of the freshwater pool core B located from the salinity barycenter within the pool compared to the Ekman velocity and wind stress at the barycenter from 1 September to 1 November 2021.

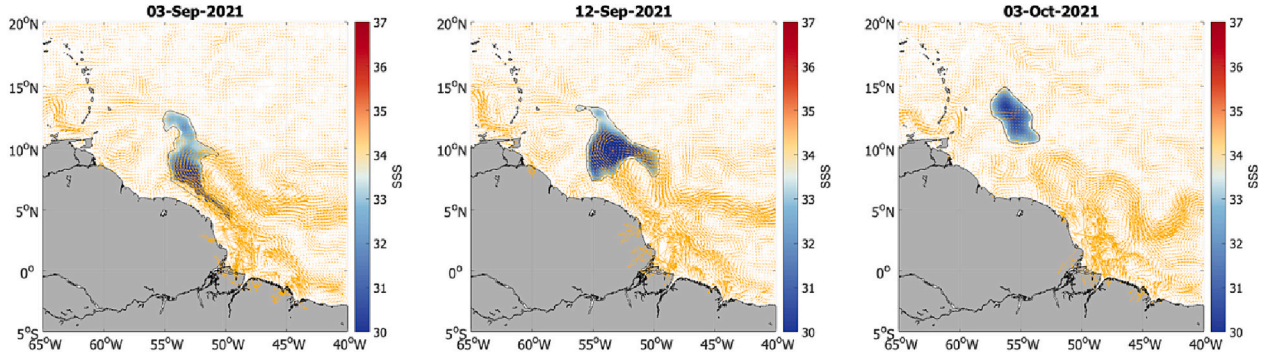

Fig. 9. Freshwater pool B identified by the 33.5 pss salinity contour for 3 September (left), 12 September (center) and 3 October (right) 2021. Background colors inside the contour indicate the surface salinity, and yellow arrows represent the geostrophic currents. (For interpretation of the references to color in this figure legend, the reader is referred to the web version of this article.)

imagery until late October near 16°N/57°W.

The speed at which the patch moved varies in a consistent way with changes in the wind stress and expected Ekman response a day or two later (Fig. 8). The Ekman current explains a large part of these variations, coherent with MLD initially on the order of 10 m or less, but which might have deepened to 15 m in early October and to close to 20 m in mid to late October, as suggested by Argo profiles located in the patch (data not shown). In addition, the underlying geostrophic current structures influenced the variability of the patch, even after the initial period of interaction with the NBC ring.

An indicator of the freshwater pool core area is reported by the area contained within the 33.5 pss salinity contour (Fig. 7). After formation, the freshwater pool core area reaches up 250.000 km^2, and decreases to 180.000 km^2 following the expulsion of a filament around the NBC ring.

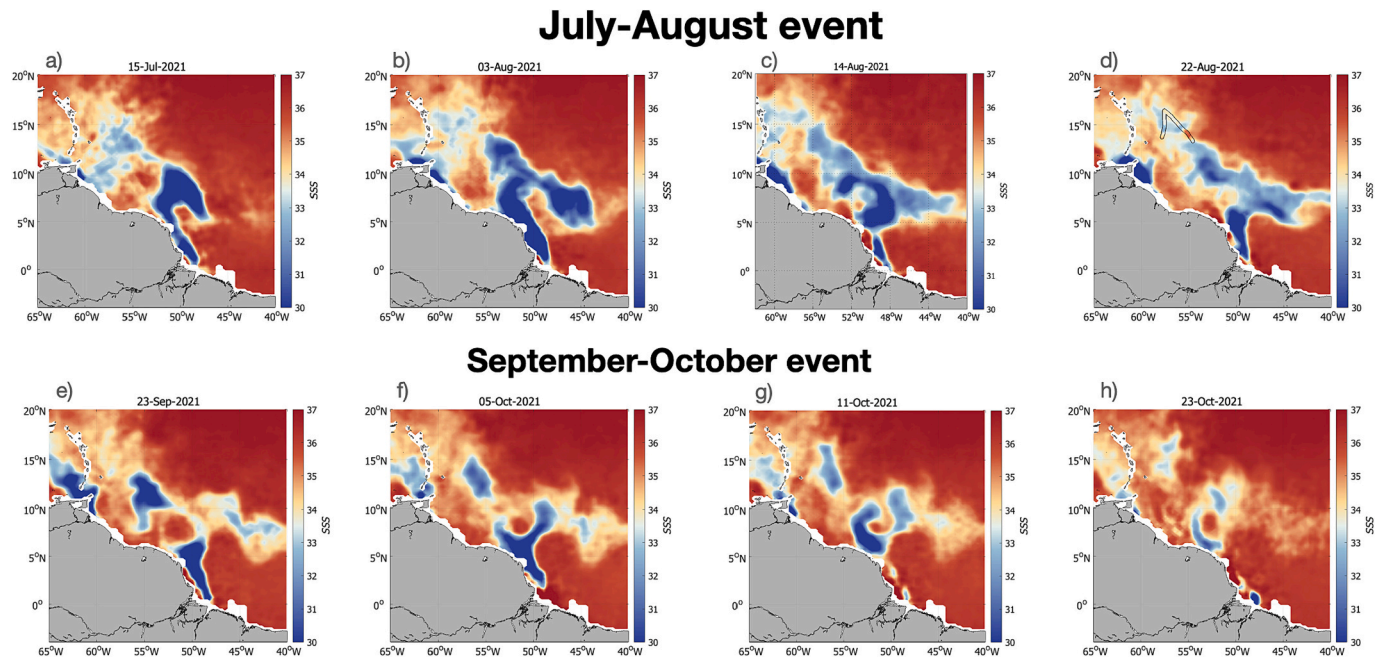

Fig. 10. SSS snapshots showing the evolution of the Amazon River plume in late July–August (top) and in late September–October (bottom). On panel d), SV Tara's track is color-coded with the salinity from the ship's TSG (see Supplementary Fig. S3b for a larger plot of SV Tara TSG salinity overlaying SSS).

A slower decrease over a few days took place during periods of high wind stress, in particular in early October, when saltier water was likely entrained from below. This was also the case at the end of October, when the salinity in the core became close to the threshold salinity of 33.5 pss. The average salinity (S_{mean}) as well as the lowest salinity (S_{min}) evolved in time towards higher salinity (Fig. 7). After 10 September, the periods of strong salinity change corresponded to days of larger wind stress (Fig. 8), also indicative of entrainment of salty water from below. Between 10 September and 3 October, the increase in S_{min} of nearly 7 pss, compared to an initial contrast of about 14 pss with underlying water, suggests a doubling of MLD or fresh-layer thickness. The initial freshwater thickness was on the order of 10 m on 10 September, which would result in a thickness of 20 m by 3 October. These values are coherent with the agreement between the displacement speed of the patch and the Ekman velocities, which are inversely proportional to the thickness (Fig. 8). Other processes such as lateral mixing or air-sea fluxes also contribute to the changes in S_{min}, and this increase in freshwater thickness should be considered as an upper estimate. Because the freshwater patch became more elongated after 1 November, it is likely that the spatial resolution then smears out the minimum salinity evolution (not shown).

3.4. Anticyclonic geostrophic circulation around the patch

The Spot drifter trajectories often hinted at an anticyclonic circulation around the freshwater patch, after it separated from the NBC ring influence (Fig. 6). This is also found in the geostrophic currents derived from altimetry (Fig. 9). The altimetric product has a lower resolution than the daily SSS and Chl*a* products but resolves the large scales of the fresh patch. Integrating the orthogonal currents across lines from the boundary (33.5 pss salinity contour) towards the center of the patch yields an estimate of the sea level increase at its center compared with the surrounding area. This estimate is rather uncertain, but its magnitude (integrating from the left or the top of the patch) suggests a higher sea level at the center by 14 cm on 12 September (as also found on the sea level maps). If this was uniquely associated with the steric effect of the fresh layer, the steric effect at the center would be roughly equivalent to a vertically integrated negative salinity anomaly of 140 pss*m at the center. Based on S_{min} at this date and assuming that the anomaly is relative to 36 pss, the SSS anomaly is 12 pss, so that this steric effect would correspond to a fresh layer thickness of 12 m, which is in line with the CTD measurements (Section 3.1). This anticyclonic surface circulation in the geostrophic current altimetric maps on 10–15 September was thus likely created by the fresh patch, and probably had no counterpart below it.

This well documented sequence illustrates the transient transport of freshwater to the northwestern Atlantic, during a season when freshwater transport is mostly expected towards the NECC. We will now use the satellite products to extend the investigation to the whole summer season of 2021.

3.5. Other freshwater events of the summer 2021

During the summer of 2021 (June to November), HR satellite salinity data showed further instances of interaction between the ARP and the NBC rings (Fig. 10). Although the freshwater patch B is the most striking example, the path of the ARP was regularly interrupted and influenced by the NBC rings. Close to 15°N, SV *Tara* crossed one freshwater patch on 22–23 August with SSS down to 32.5 pss. This patch seems mostly advective and not locally created, as it can be tracked back to the NBC retroflection at the beginning of July, >1.5 month earlier. The patch separated from the plume in late July following an interaction between the meandering NBC retroflection and a ring detached earlier from the retroflection (not shown). Even when the NBC retroflection is not yet in place, the presence of rings induces freshwater recirculation around them. This quickly brings the freshwater northward (about a month to reach the Lesser Antilles), therefore modifying the ARP path. Starting on 11 July, the main pathway of freshwater did not follow the bathymetry nor the shelf break near the Demerara Rise.

After the main fresh patch event end of September, the retroflection was again well-established and started to direct the new ARP towards the NECC. However, the interaction with the ring was still very complex, as part of the ARP started to recirculate around the ring on 1 October (Fig. 10 e, f). This ring recirculation and the first NECC pool merged by 23 October, surprisingly traveling northwestward and thus not rejoining the NECC (Supplementary Fig. S5).

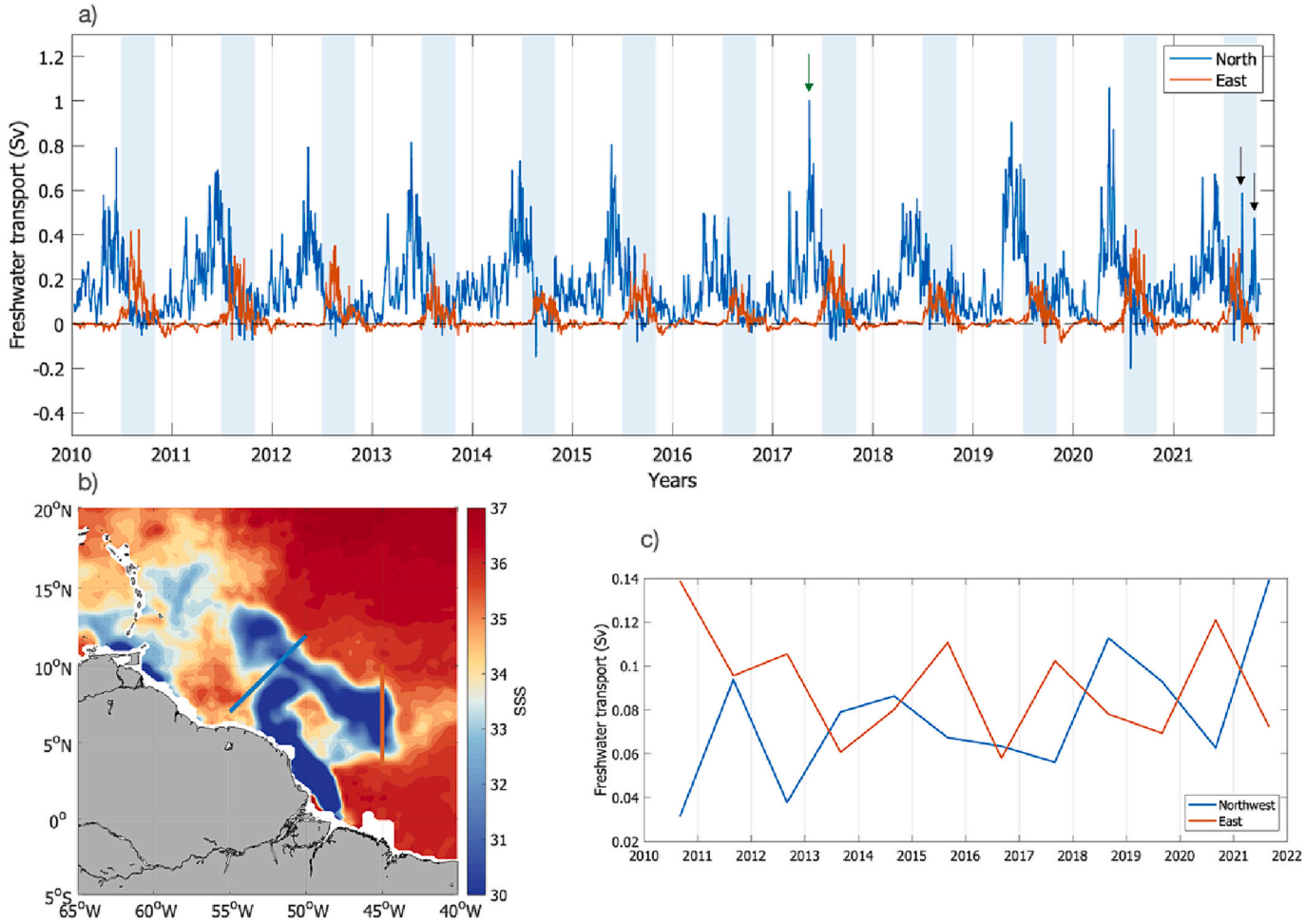

Fig. 11. a) Freshwater transport along the two sections defined on panel b. The 1 July to 1 November period is indicated by the light blue bands, the two black arrows mark the freshwater events of September and October 2021, the green arrow mark the freshwater event crossed by cyclone Irma. (b) Eastward transport is computed across the 45°W section in orange, while the northwestward transport is computed across the blue south-west/north-east section. c) Mean low frequency (30-days moving average) eastward and northwestward transport averaged for the months of August–September-October of each year. (For interpretation of the references to color in this figure legend, the reader is referred to the web version of this article.)

3.6. Interannual variability

Summertime ARP – NBC rings interactions are common in the northwestern tropical Atlantic from 2010 to 2021, inducing an alternating freshwater transport between a northwestward and an eastward direction. However, in this record, each transport event is unique, and none is as striking and well defined as the fresh patch B studied in this paper. To find how these mesoscale structures contribute to the total freshwater transport and its interannual variability, the northwestward and eastward transports (described in section 2.5.2) are estimated. The eastward transport is computed across a 45°W section between 4°N and 10°N. The northwestward transport is evaluated through a diagonal section presented on Fig. 11b, which is to the northwest of where eddies usually form and separate from the NBC retroflection. A 14 m freshwater thickness is assumed, based on stations 35 and 36a out of the plume, on the TIA sections and on Argo profiles located in this region in summer (not shown) to compute Ekman velocities from satellite wind stress and to vertically integrate the transport.

The year 2021 is unique for northwestward freshwater transport in late summer due to the two strong events presented above (Fig. 11). The September 2021 patch B contributes to 25% of the northwestward transport over the July–November 2021 period. The northward transport in late summer also happens during short-lived and intense events as in 2011, 2014, 2016, 2018 and to a lesser extent in 2019. For these years, eastward transport in the NECC is also rather intermittent, and smaller events of northward transport appear after September in 2014, 2018 and 2019. There is an episodic switching between northward and eastward transport supported by the strong anti-correlation (−0.85) between the mean low-frequency (30-days moving average) eastward and northwestward transport for the months of August–September-October (*Fig. 11*c).

4. Discussion

4.1. Observing rapidly varying SSS from space

For the sake of reducing noise on satellite SSS, most level 3–4 products are smoothed over a week/month and ~ 70 km. Here, we observed from chlorophyll-a and in-situ SSS data a high degree of variability on temporal scales smaller than a week that have a significant impact on the plume dynamics. We show that this temporal scale (day-to-day) can be better resolved from current SMOS/SMAP measurement with less temporally smoothed products. There is therefore an interest in generating products with a higher resolution than the week. The exponential time correlation kernel used in the OI was chosen to give a higher weight to the data closest to the date of interest than a Gaussian kernel. This choice was somewhat arbitrary, although it gives reasonable results. In the HR product, we chose to improve the temporal resolution

but not the spatial resolution. Given the native spatial resolution of SMOS and SMAP, it is possible to achieve a spatial resolution of 50 km, as was done in the original 'manually' made product during the SMOS-SMAP period. However, this is at the expense of the SSS noise which is particularly important during the SMOS-only period (2010–2015). In the region investigated, the time resolution gain seen with the HR product is very close to the one seen with the original 'manually' made product because time evolution is fast and dominates the SSS variability, hence validating a posteriori our choice. Observing rapidly (from day to day) varying SSS structures from space is therefore currently possible when the SSS variability is strong, with contrasted structures. It nevertheless shows the need for higher spatial and temporal resolution SSS product for all the regions that are either smaller or not as contrasted as the river estuaries (NECC further away from the plume…).

4.2. A new summer ARP pathway

This study shows that the ARP cannot be treated as a coherent structure, in agreement with the conclusions of Coles et al. (2013). The ARP strongly interacts with its environment, and in particular with the NBC retroflection, the NBC rings, and the local winds. Molleri et al. (2010) identified three plume pathways, the dominant pathway from August to November being eastward towards the NECC. Based on a model study, Coles et al. (2013) identified four pathways, only one of which, found mostly in winter, the "interior gyre pathway", involves a prevailing Ekman transport. They also identified another northwestward pathway, the "direct northwestward pathway", described as particles advected rapidly northwestward, either through the Guyana coastal Current or further away from the coast. The trajectories of particles in this pathway are less looped compared to the transport through the NBC rings associated with the 'indirect northwest pathway' (Coles et al., 2013).

Our observations suggest that this 'indirect northwestward' pathway is present all year-around, and not only in winter. In late summer, we even find it to be one of the dominant pathways. This pathway is strongly driven by Ekman transport when the geostrophic currents do not favor this pathway once the retroflection is established, explaining the rapid water transport. The pathway is mainly discontinuous and is the main pathway bringing freshwater to the northwestern tropical Atlantic in summer and autumn. Without rings, the plume would likely either be transported by the NBC then the Guyana coastal current along the shelf break, or follow the NBC retroflection and join the NECC. The strong geostrophic circulation associated with the NBC rings entrains the plume out of the main currents of the region. In doing so, the rings do not directly transport freshwater but create the alternative pathway from the Demerara Rise (~55°W) towards the northwest, that can either be semi-continuous or completely patchy.

This study emphasizes the strong role of Ekman velocities in the total northwestward transport of freshwater. However, the estimated freshwater transport in section 3.6 highlights uncertainties due to the assumption that salinity is homogeneous over the Ekman layer and that the Ekman and geostrophic currents transport the surface salinity anomaly. The Ekman transport at 90° of the wind direction is an integration of the currents of the Ekman spiral over the Ekman layer. However, the Ekman layer could extend deeper than the low salinity layer, through the vertical salinity gradient. In this case, the direction of the transport of the lower surface salinities would be advected in a direction closer to the wind direction, whereas the Ekman currents at play in the deeper layers, which are saltier, would contribute less to the freshwater transport. Uncertainty also arises due to the Ekman layer depth, chosen here at 14 m. Several sensitivity tests have been conducted with different depths, and a change of ±5 m leads to a change of the freshwater transport of <0.1 Sv for the 2021 event presented in this paper. In addition, geostrophic currents are subject to uncertainties due to the smoothing of the altimetric product both in time and space. Furthermore, the salinity products do not resolve structures smaller than 70 km such as some of the filaments featured in the chlorophyll maps.

4.3. Interannual variability

Over the last 11 years, interannual variability of the eastward and northwestward freshwater transport is observed in late summer (*Fig. 11*c). At least four processes are responsible for the variability of this transport.

First, the upper geostrophic circulation has been shown to be one of the main sources of interannual variability in the western tropical Atlantic (Da and Foltz, 2022; Jouanno et al., 2017; Masson and Delecluse, 2001). Once the intertropical convergence zone reaches latitudes higher than 9°N in July, it drives the retroflection of the NBC to feed the invigorated NECC. There is however interannual variations in the intensity of the NECC and in the establishment of the retroflection that strongly influences the ARP extension (Da and Foltz, 2022). In 2011, 2014 and 2016, the NBC started retroflecting later than usual. This led to a longer period of northwestward transport and weaker total export towards the NECC. On the other hand, an early onset of the NBC retroflection such as in 2017, 2020 and 2021 favored the development of eastward-extending freshwater patches.

Second, the detachment of patches from the main ARP is often driven by NBC rings. In July 2021 the ARP and two NBC rings interacted, while the September event was due to a single ring. In summer the rings move more slowly and stay longer in the Demerara Rise region than in other seasons (Aroucha et al., 2020) as observed in 2021, but with some variability from year to year. The number of rings also varies interannually (Aroucha et al., 2020), modifying the ARP-ring interactions and therefore the shape of the plume. As a ring forms, the retroflection extends northward (up to 10°N), a position that might favor northwestward transport, especially if the ring circulation is intense. Once the ring is shed, the retraction of the retroflection to its southeasternmost position (~5°N) favors direct eastward transport.

Third, as the fresh layer is often <10-m thick, winds play a major role in driving its spatial distribution. We showed here the prominent role of Ekman currents over the northwestward spreading of ARP and associated freshwater transport in summer. This supports how the overall shape of the plume strongly varies under the influence of winds between 2012 and 2014 as observed by Fournier et al. (2017). When investigating the variability of the freshwater transport in the NECC, Grodsky et al. (2022) also pointed out the strong correlation between SSS anomalies propagating in the NECC and winds.

Finally, the Amazon outflow variability modulates the low-frequency (1-year moving average) total freshwater transport (correlation of 0.75, Supplementary Fig. S6). The most visible impact of the Amazon outflow on the freshwater transport is observed in 2016, when the very low flow (0.13 Sv) of the Amazon following the El Niño event of 2015 clearly results in both weak northwestward and eastward transports. Gévaudan et al. (2022) showed the stronger impacts of extreme floods and droughts of the Amazon River on SSS variability. Moreover, Tyaquiçã et al. (2017) found that the SSS of the northwestern tropical Atlantic Ocean can be driven by Pacific SST patterns, and that the magnitude of the SSS anomaly varies according to the magnitude and frequency of El Niño Modoki events.

5. Conclusion

The 'Microbiomes' cruise onboard SV *Tara* in late summer of 2021 crossed a very discontinuous ARP. The layer with a strong surface freshening from the Amazon outflow is very stratified even 1000 km away from the estuary (pycnocline at ~15 m) and is often associated with intense surface currents. Based on these observations highlighting the small spatial and temporal scales of ARP, we demonstrate the ability of a new high temporal resolution satellite SSS product, combined with chlorophyll-a and altimetry, to interpret ARP dynamics.

The altimetry data coupled to drifter trajectories illustrate the role of

the NBC retroflection and of a newly formed NBC ring in driving the ARP. This ring was stationary and remained in the retroflection region until the end of October. At the beginning of September, the plume expanded rapidly and was entrained on the western periphery of the ring. The ring collided with the shelf and cut off the freshwater source, creating a 200,000 km^2 freshwater patch northwest of the ring. Under the action of the winds and therefore of the Ekman currents, this patch did not completely recirculate around the ring but moved to the northwest towards the Lesser Antilles. It was identifiable by salinities lower than 33.5 pss until early November. This structure was very stratified, and once detached from the influence of the ring, mainly driven by sheared Ekman currents. The strong steric anomaly associated with the freshwater patch generated an anticyclonic circulation around the patch, well identified by altimetric currents.

This process offers an alternative path to the transport of freshwater towards the NECC, which is favored when the retroflection of the NBC is in place. Within the whole summer 2021, the event described above is a particularly strong case, but not isolated. As early as in July, a fragmentation of the plume due to interactions with the rings was observed. This is also the case later in October–November during a period of lower Amazon outflow.

The calculation of freshwater transport towards the northwest (Caribbean) and towards the east (NECC) showed a succession of distinct events of varying intensity, with shifts between the two directions of transport. A larger than average northwestward transport is observed in late summer 2021, linked to these events dominated by Ekman transport. Over the period 2010–2021, for each summer, most of the transport happened during distinct events, but few were as well defined as the one sampled by the SV *Tara* in September 2021.

In conclusion, the Amazon plume is not only driven by the large-scale currents prevailing in the region. The Guiana Current and the retroflection-NECC system certainly carry a lot of freshwater, but the almost unavoidable interaction with the NBC rings close to 55°W generates alternative pathways. These events are intermittent, but intense, and contribute to the spatial distribution of salinity and barrier layers in the tropical Atlantic.

The oceanic mesoscale plays therefore a key role in the export of freshwater from river plumes. Observing the day-to-day SSS variability at mesoscale from space is challenging, but this study shows the ability of the new CATDS HR product to well resolve it. In particular it succeeded in tracking the formation a mesoscale freshwater patch, and following it over more than a month. This is an important step forward for the study of all regions with high SSS variability, such as the Gulf of Mexico and the Brazil-Falklands confluence zone, to name but a few examples. The smaller spatial scales revealed by the high-resolution chlorophyll-a also suggest many finer scale features that also contribute to transport, showing the need for higher spatial resolution satellite salinity products.

Knowing the Amazon freshwater spreading history is important for the study of TC that often cross low salinity areas near the Caribbean (eg., Balaguru et al., 2020; Reul et al., 2021). Moreover, the waters of the Amazon are rich in nutrients, generate high primary production and are associated with a rich biodiversity and carbon drawdown (Neumann-Leitão et al., 2018; Smith and Demaster, 1996). Better defining the dispersal pathways of these waters therefore has strong consequences for the supply of nutrients to the tropical Atlantic with a preference for the central or the northwestern Atlantic. The magnitude of the air-sea CO_2 fluxes recorded in the northwestern tropical Atlantic considerably varies from year to year and from region to region (e.g. Ibánhez et al., 2015; Lefévre et al., 2010; Louchard et al., 2021). Investigating the link between the variability of freshwater and air-sea CO_2 fluxes is therefore important for understanding the carbon sink associated to the Amazon plume waters.

Open research

We benefited from numerous data sets made freely available and listed here: the currents produced by Ssalto/Duacs distributed by the CMEMS (https://resources.marine.copernicus.eu), the Chl*a* maps produced by CLS (https://datastore.cls.fr/catalogues/chlorophyll-high-resolution). The Argo data collected are made freely available by the International Argo Program and the national programs that contribute to it (http://doi.org/10.17882/42182). The CEC CATDS High Resolution V0 Sea Surface Salinity maps produced by LOCEAN/IPSL (UMR CNRS/UPMC/IRD/MNHN) laboratory and ACRI-st company that participate to the Ocean Salinity Expertise Center (CECOS) of Centre Aval de Traitement des Données SMOS (CATDS) (doi: 10.17882/90082). The SPOT data deployed from SV Tara are available on PANGEA (doi: https://doi.org/10.1594/pangaea.948244) and so are the towed instrument array data (https://doi.pangaea.de/10.1594/PANGAEA.953830). The CTD and TSG data used in this study are available on Zenodo (doi:https://doi.org/10.5281/zenodo.7528491). They will also be made available at a later date on seanoe together with all the data from the Microbiomes AtlantECO cruise.

CRediT authorship contribution statement

L. Olivier: Writing – review & editing, Writing – original draft, Visualization, Validation, Methodology, Investigation, Formal analysis, Data curation, Conceptualization. **G. Reverdin:** Writing – review & editing, Supervision, Funding acquisition, Conceptualization. **J. Boutin:** Writing – review & editing, Supervision, Funding acquisition, Conceptualization. **R. Laxenaire:** Writing – review & editing, Resources, Methodology. **D. Iudicone:** Project administration, Funding acquisition. **S. Pesant:** Resources, Project administration, Funding acquisition. **Paulo H.R. Calil:** Writing – review & editing, Resources, Project administration, Funding acquisition. **J. Horstmann:** Resources, Project administration, Funding acquisition. **D. Couet:** Resources, Data curation. **J.M. Erta:** Resources, Data curation. **P. Huber:** Writing – review & editing, Resources, Data curation. **H. Sarmento:** Writing – review & editing, Project administration, Funding acquisition. **A. Freire:** Resources, Data curation. **A. Koch-Larrouy:** Writing – review & editing, Funding acquisition, Data curation. **J.-L. Vergely:** Validation, Resources, Methodology, Data curation. **P. Rousselot:** Resources, Data curation. **S. Speich:** Writing – review & editing, Supervision, Resources, Project administration, Funding acquisition.

Declaration of competing interest

The authors declare that they have no known competing financial interests or personal relationships that could have appeared to influence the work reported in this paper.

Data availability

Data will be made available on request.

Acknowledgments

We wish to thank the Tara Ocean Foundation, the SV *Tara* crew and all those who participated in Mission Microbiomes AtlantECO. This publication has received funding from the European Union's Horizon 2020 research and innovation program under grant agreement No 862923 (project AtlantECO), with additional support from CNES (the French National Center for Space Studies) through the TOSCA SMOS-Ocean and TOEddies proposals. This output reflects only the author's view and the European Union cannot be held responsible for any use that may be made of the information contained therein. We warmly thank M. Heineke, Thomas Kock and Rolf Riethmüller (Hereon research centre) for processing the TIA data. LO was supported by a scholarship from the

Ecole Normale Supérieure. This work was supported by the Initiative and Networking Fund of the Helmholtz Association (Grant Number: VH-NG-19-33). We thank the Fondation Tara Ocean and in particular R. Troublé, C. Moulin and A. Bourdais for making the Mission Microbiomes happen. Thank you to all the SV *Tara* leg 5 crew members, M. Hertau, N. Bin, L. Caudan, S. Bin, F. Aurat and A. Prieur for their precious help in conducting the science onboard. Thank you to M. Labaste for analyzing the salinity samples, and to C. Guillerm and Météo-France for providing the 10 SVP drifters. We are keen to acknowledge the commitment of the following institutions for their financial and scientific support that made Mission Microbiomes AtlantECO possible: Stazione Zoologica Anton Dohrn, European Bioinformatics Institute (EMBL-EBI), Centre national de la recherche scientifique (CNRS), Centre National de Séquençage (CNS, Genoscope), agnès b., UNESCO-IOC, the Veolia Foundation, the Prince Albert II de Monaco Foundation, Région Bretagne, Billerudkorsnas, AmerisourceBergen Company, Lorient Agglomération, Oceans by Disney, L'Oréal, Biotherm, France Collectivités, Fonds Français pour l'Environnement Mondial, and Etienne Bourgois.

Appendix A. Supplementary data

Supplementary data to this article can be found online at https://doi.org/10.1016/j.rse.2024.114165.

References

Aroucha, L.C., Veleda, D., Lopes, F.S., Tyaquiçã, P., Lefèvre, N., Araujo, M., 2020. Intra- and inter-annual variability of North Brazil current rings using angular momentum Eddy detection and tracking algorithm: observations from 1993 to 2016. J. Geophys. Res. Oceans 125, e2019JC015921. https://doi.org/10.1029/2019JC015921.

Balaguru, K., Chang, P., Saravanan, R., Leung, L.R., Xu, Z., Li, M., Hsieh, J.-S., 2012. Ocean barrier layers' effect on tropical cyclone intensification. Proc. Natl. Acad. Sci. 109, 14343–14347. https://doi.org/10.1073/pnas.1201364109.

Balaguru, K., Foltz, G.R., Leung, L.R., Kaplan, J., Xu, W., Reul, N., Chapron, B., 2020. Pronounced impact of salinity on rapidly intensifying tropical cyclones. Bull. Am. Meteorol. Soc. 101, E1497–E1511. https://doi.org/10.1175/BAMS-D-19-0303.1.

Bertrand, A., Emmanuel, De Saint Leger, Ariane, Koch-Larrouy, 2021. AMAZOMIX 2021 cruise,Antea R/V. https://doi.org/10.17600/18001364.

Boutin, J., Chao, Y., Asher, W.E., Delcroix, T., Drucker, R., Drushka, K., Kolodziejczyk, N., Lee, T., Reul, N., Reverdin, G., Schanze, J., Soloviev, A., Yu, L., Anderson, J., Brucker, L., Dinnat, E., Santos-Garcia, A., Jones, W.L., Maes, C., Meissner, T., Tang, W., Vinogradova, N., Ward, B., 2016. Satellite and in situ salinity: understanding near-surface stratification and subfootprint variability. Bull. Am. Meteorol. Soc. 97, 1391–1407. https://doi.org/10.1175/BAMS-D-15-00032.1.

Boutin, Jacqueline, Vergely Jean-Luc, Olivier, Léa, Reverdin Gilles, Perrot Xavier, 2022. SMOS SMAP High Resolution SSS maps in regions of high variability, generated by CATDS CEC. SEANOE. Thouvenin-Masson Clovis. https://doi.org/10.17882/90082.

Boutin, J., Vergely, J.-L., Marchand, S., d'Amico, F., Hasson, A., Kolodziejczyk, N., Reul, N., Reverdin, G., Vialard, J., 2018. New SMOS Sea surface salinity with reduced systematic errors and improved variability. Remote Sens. Environ. 214, 115–134.

Boutin, J., Reul, N., Koehler, J., Martin, A., Catany, R., Guimbard, S., Rouffi, F., Vergely, J.L., Arias, M., Chakroun, M., Corato, G., Estella-Perez, V., Hasson, A., Josey, S., Khvorostyanov, D., Kolodziejczyk, N., Mignot, J., Olivier, L., Reverdin, G., Stammer, D., Supply, A., Thouvenin-Masson, C., Turiel, A., Vialard, J., Cipollini, P., Donlon, C., Sabia, R., Mecklenburg, S., 2021. Satellite-based sea surface salinity designed for ocean and climate studies. J. Geophys. Res. Oceans 126, e2021JC017676. https://doi.org/10.1029/2021JC017676.

Chaudhuri, D., Sengupta, D., D'Asaro, E., Shivaprasad, S., 2021. Trapping of wind momentum in a Salinity-Stratified Ocean. J. Geophys. Res. Oceans 126, e2021JC017770. https://doi.org/10.1029/2021JC017770.

Coles, V.J., Brooks, M.T., Hopkins, J., Stukel, M.R., Yager, P.L., Hood, R.R., 2013. The pathways and properties of the Amazon River plume in the tropical North Atlantic Ocean. J. Geophys. Res. Oceans 118, 6894–6913. https://doi.org/10.1002/2013JC008981.

Da, N.D., Foltz, G.R., 2022. Interannual variability and multiyear trends of sea surface salinity in the Amazon-orinoco plume region from satellite observations and an ocean reanalysis. J. Geophys. Res. Oceans 127, e2021JC018366. https://doi.org/10.1029/2021JC018366.

Dai, A., Trenberth, K.E., 2002. Estimates of freshwater discharge from continents: latitudinal and seasonal variations. J. Hydrometeorol. 3, 660–687. https://doi.org/10.1175/1525-7541(2002)003<0660:EOFDFC>2.0.CO;2.

Dai, A., Qian, T., Trenberth, K.E., Milliman, J.D., 2009. Changes in continental freshwater discharge from 1948 to 2004. J. Clim. 22, 2773–2792. https://doi.org/10.1175/2008JCLI2592.1.

de Boyer Montégut, C., Madec, G., Fischer, A.S., Lazar, A., Iudicone, D., 2004. Mixed layer depth over the global ocean: an examination of profile data and a profile-based climatology. J. Geophys. Res. Oceans 109. https://doi.org/10.1029/2004JC002378.

Ferry, N., Reverdin, G., 2004. Sea surface salinity interannual variability in the western tropical Atlantic: an ocean general circulation model study. J. Geophys. Res. Oceans 109. https://doi.org/10.1029/2003JC002122.

Ffield, A., 2005. North Brazil current rings viewed by TRMM microwave imager SST and the influence of the Amazon plume. Deep Sea Res. Part Oceanogr. Res. Pap. 52, 137–160. https://doi.org/10.1016/j.dsr.2004.05.013.

Ffield, A., 2007. Amazon and Orinoco River plumes and NBC rings: bystanders or participants in hurricane events? J. Clim. 20, 316–333. https://doi.org/10.1175/JCLI3985.1.

Foltz, G.R., McPhaden, M.J., 2009. Impact of barrier layer thickness on SST in the central tropical North Atlantic. J. Clim. 22, 285–299. https://doi.org/10.1175/2008JCLI2308.1.

Fournier, S., Chapron, B., Salisbury, J., Vandemark, D., Reul, N., 2015. Comparison of spaceborne measurements of sea surface salinity and colored detrital matter in the Amazon plume. J. Geophys. Res. Oceans 120, 3177–3192. https://doi.org/10.1002/2014JC010109.

Fournier, S., Vandemark, D., Gaultier, L., Lee, T., Jonsson, B., Gierach, M.M., 2017. Interannual variation in offshore advection of Amazon-Orinoco plume waters: observations, forcing mechanisms, and impacts. J. Geophys. Res. Oceans 122, 8966–8982. https://doi.org/10.1002/2017JC013103.

Fratantoni, D.M., Glickson, D.A., 2002. North Brazil current ring generation and evolution observed with SeaWiFS. J. Phys. Oceanogr. 32, 1058–1074. https://doi.org/10.1175/1520-0485(2002)032<1058:NBCRGA>2.0.CO;2.

Gévaudan, M., Durand, F., Jouanno, J., 2022. Influence of the Amazon-Orinoco discharge interannual variability on the Western tropical Atlantic salinity and temperature. J. Geophys. Res. Oceans 127, e2022JC018495. https://doi.org/10.1029/2022JC018495.

Goni, G.J., Johns, W.E., 2001. A census of North Brazil current rings observed from TOPEX/POSEIDON altimetry: 1992–1998. Geophys. Res. Lett. 28, 1–4. https://doi.org/10.1029/2000GL011717.

Grodsky, S.A., Reul, N., Lagerloef, G., Reverdin, G., Carton, J.A., Chapron, B., Quilfen, Y., Kudryavtsev, V.N., Kao, H.-Y., 2012. Haline hurricane wake in the Amazon/Orinoco plume: AQUARIUS/SACD and SMOS observations. Geophys. Res. Lett. 39 https://doi.org/10.1029/2012GL053335.

Grodsky, S.A., Reul, N., Bentamy, A., Vandemark, D., 2022. Eastward propagating surface salinity anomalies in the tropical North Atlantic. Remote Sens. Lett. 13, 334–342. https://doi.org/10.1080/2150704X.2022.2032452.

Hersbach, H., Bell, B., Berrisford, P., Biavati, G., Horányi, A., Muñoz Sabater, J., Nicolas, J., Peubey, C., Radu, R., Rozum, I., 2018. ERA5 hourly data on single levels from 1979 to present. Copernic. Clim. Change Serv. C3s Clim. Data Store Cds 10.

IAPSO Working Group on Symbols, U, N. in P.O. (SUN), 1985. The international system of units (SI). In: Oceanography: Report of IAPSO Working Group on Symbols, Units and Nomenclature in Physical Geography (SUN). Unesco.

Ibánhez, J.S.P., Diverrès, D., Araujo, M., Lefèvre, N., 2015. Seasonal and interannual variability of sea-air CO2 fluxes in the tropical Atlantic affected by the Amazon River plume. Glob. Biogeochem. Cycles 29, 1640–1655. https://doi.org/10.1002/2015GB005110.

Johns, W.E., Lee, T.N., Schott, F.A., Zantopp, R.J., Evans, R.H., 1990. The North Brazil current retroflection: seasonal structure and eddy variability. J. Geophys. Res. Oceans 95, 22103–22120. https://doi.org/10.1029/JC095iC12p22103.

Johns, W.E., Zantopp, R.J., Goni, Gustavo J., 2003. Cross-gyre transport by North Brazil Current rings. In: Goni, G.J., Malanotte-Rizzoli, P. (Eds.), Elsevier Oceanography Series, Interhemispheric Water Exchange in the Atlantic Ocean. Elsevier, pp. 411–441. https://doi.org/10.1016/S0422-9894(03)80156-3.

Jouanno, J., Hernandez, O., Sanchez-Gomez, E., 2017. Equatorial Atlantic interannual variability and its relation to dynamic and thermodynamic processes. Earth Syst. Dynam. 8, 1061–1069. https://doi.org/10.5194/esd-8-1061-2017.

Kock, T., Baschek, B., Wobbe, F., Heineke, M., Riethmueller, R., Deschner, S.C., Seidel, G., Calil, P.H.R., 2023. An advanced towed CTD chain for physical-biological high resolution in situ upper ocean measurements. Front. Mar. Sci. 10.

Laxenaire, R., Speich, S., Blanke, B., Chaigneau, A., Pegliasco, C., Stegner, A., 2018. Anticyclonic Eddies connecting the Western Boundaries of Indian and Atlantic Oceans. J. Geophys. Res. Oceans 123, 7651–7677. https://doi.org/10.1029/2018JC014270.

Lefévre, N., Diverrés, D., Gallois, F., 2010. Origin of CO2 undersaturation in the western tropical Atlantic. Tellus Ser. B Chem. Phys. Meteorol. 62, 595–607. https://doi.org/10.1111/j.1600-0889.2010.00475.x.

Louchard, D., Gruber, N., Münnich, M., 2021. The impact of the Amazon on the biological pump and the Air-Sea CO2 balance of the Western Tropical Atlantic. Glob. Biogeochem. Cycles 35, e2020GB006818. https://doi.org/10.1029/2020GB006818.

Lumpkin, R., Pazos, M., 2007. Measuring surface currents with surface velocity program drifters: the instrument, its data, and some recent results. Lagrangian Anal. Predict. Coast. Ocean Dyn. 39, 67.

Masson, S., Delecluse, P., 2001. Influence of the Amazon River runoff on the tropical atlantic. Phys. Chem. Earth Part B Hydrol. Oceans Atmos. 26, 137–142. https://doi.org/10.1016/S1464-1909(00)00230-6.

Mélice, J.-L., Arnault, S., 2017. Investigation of the intra-annual variability of the north equatorial countercurrent/North Brazil current eddies and of the instability waves of the north tropical Atlantic Ocean using satellite altimetry and empirical mode decomposition. J. Atmos. Ocean. Technol. 34, 2295–2310. https://doi.org/10.1175/JTECH-D-17-0032.1.

Molleri, G.S.F., de Novo, E.M.L.M., Kampel, M., 2010. Space-time variability of the Amazon River plume based on satellite ocean color. Cont. Shelf Res. 30, 342–352. https://doi.org/10.1016/j.csr.2009.11.015.

Muller-Karger, F.E., McClain, C.R., Richardson, P.L., 1988. The dispersal of the Amazon's water. Nature 333, 56–59. https://doi.org/10.1038/333056a0.

Neumann-Leitão, S., Melo, P.A.M.C., Schwamborn, R., Diaz, X.F.G., Figueiredo, L.G.P., Silva, A.P., Campelo, R.P.S., de Melo Júnior, M., Melo, N.F.A.C., Costa, A.E.S.F., Araújo, M., Veleda, D.R.A., Moura, R.L., Thompson, F., 2018. Zooplankton from a reef system under the influence of the Amazon River Plume. Front. Microbiol. 9.

Niiler, P.P., Paduan, J.D., 1995. Wind-driven motions in the Northeast Pacific as measured by Lagrangian drifters. J. Phys. Oceanogr. 25, 2819–2830.

Oliva, R., Daganzo, E., Richaume, P., Kerr, Y., Cabot, F., Soldo, Y., Anterrieu, E., Reul, N., Gutierrez, A., Barbosa, J., Lopes, G., 2016. Status of radio frequency interference (RFI) in the 1400–1427MHz passive band based on six years of SMOS mission. Remote Sens. Environ., Special Issue: ESA's Soil Moisture Ocean Salinity Mission - Achieve. Appl. 180, 64–75. https://doi.org/10.1016/j.rse.2016.01.013.

Olivier, L., Boutin, J., Reverdin, G., Lefèvre, N., Landschützer, P., Speich, S., Karstensen, J., Labaste, M., Noisel, C., Ritschel, M., Steinhoff, T., Wanninkhof, R., 2022. Wintertime process study of the North Brazil current rings reveals the region as a larger sink for CO_2 than expected. Biogeosciences 19, 2969–2988. https://doi.org/10.5194/bg-19-2969-2022.

Olivier, L., Reverdin, G., Pesant, S., Iudicone, D., 2023. CTD data from leg 5 and thermosalinograph data from legs 5,6,7 of Mission microbiomes AtlantECO on board SV Tara. Zenodo. https://doi.org/10.5281/zenodo.7528491.

Pedlosky, J., 2012. Geophysical Fluid Dynamics. Springer Science & Business Media.

Pottier, C., Garcon, V., Larnicol, G., Sudre, J., Schaeffer, P., Le Traon, P.-Y., 2006. Merging SeaWiFS and MODIS/Aqua Ocean color data in north and equatorial Atlantic using weighted averaging and objective analysis. IEEE Trans. Geosci. Remote Sens. 44, 3436–3451. https://doi.org/10.1109/TGRS.2006.878441.

Poulain, P.-M., Centurioni, L., Özgökmen, T., 2022. Comparing the currents measured by CARTHE, CODE and SVP drifters as a function of wind and wave conditions in the southwestern Mediterranean Sea. Sensors 22, 353. https://doi.org/10.3390/s22010353.

Reul, N., Fournier, S., Boutin, J., Hernandez, O., Maes, C., Chapron, B., Alory, G., Quilfen, Y., Tenerelli, J., Morisset, S., Kerr, Y., Mecklenburg, S., Delwart, S., 2014. Sea surface salinity observations from space with the SMOS satellite: a new means to monitor the marine branch of the water cycle. Surv. Geophys. 35, 681–722. https://doi.org/10.1007/s10712-013-9244-0.

Reul, N., Grodsky, S.A., Arias, M., Boutin, J., Catany, R., Chapron, B., d'Amico, F., Dinnat, E., Donlon, C., Fore, A., 2020. Sea surface salinity estimates from spaceborne L-band radiometers: an overview of the first decade of observation (2010–2019). Remote Sens. Environ. 242, 111769.

Reul, N., Chapron, B., Grodsky, S.A., Guimbard, S., Kudryavtsev, V., Foltz, G.R., Balaguru, K., 2021. Satellite observations of the sea surface salinity response to tropical cyclones. Geophys. Res. Lett. 48, e2020GL091478 https://doi.org/10.1029/2020GL091478.

Reverdin, G., Olivier, L., Foltz, G.R., Speich, S., Karstensen, J., Horstmann, J., Zhang, D., Laxenaire, R., Carton, X., Branger, H., Carrasco, R., Boutin, J., 2021. Formation and evolution of a freshwater plume in the northwestern tropical Atlantic in February 2020. J. Geophys. Res. Oceans 126, e2020JC016981. https://doi.org/10.1029/2020JC016981.

Reverdin, G., Olivier, L., Cabanes, C., Boutin, J., Thouvenin-Masson, C., Vergely, J.-L., Kolodziejczyk, N., Thierry, V., Khvorostyanov, D., Jouanno, J., 2024. Missing argo float profiles in highly stratified waters of the Amazon river plume. J. Atmos. Ocean. Technol., 41(3), 221-233.

Richardson, P.L., Hufford, G.E., Limeburner, R., Brown, W.S., 1994. North Brazil current retroflection eddies. J. Geophys. Res. Oceans 99, 5081–5093. https://doi.org/10.1029/93JC03486.

Saha, A., Serra, N., Stammer, D., 2021. Growth and decay of northwestern tropical Atlantic barrier layers. J. Geophys. Res. Oceans 126. https://doi.org/10.1029/2020JC016956.

Salisbury, J., Vandemark, D., Campbell, J., Hunt, C., Wisser, D., Reul, N., Chapron, B., 2011. Spatial and temporal coherence between Amazon River discharge, salinity, and light absorption by colored organic carbon in western tropical Atlantic surface waters. J. Geophys. Res. Oceans 116. https://doi.org/10.1029/2011JC006989.

Smith, W.O., Demaster, D.J., 1996. Phytoplankton biomass and productivity in the Amazon River plume: correlation with seasonal river discharge. Cont. Shelf Res. 16, 291–319. https://doi.org/10.1016/0278-4343(95)00007-N.

Steinmetz, F., Deschamps, P.-Y., Ramon, D., 2011. Atmospheric correction in presence of sun glint: application to MERIS. Opt. Express 19, 9783–9800.

Subramaniam, A., Yager, P.L., Carpenter, E.J., Mahaffey, C., Björkman, K., Cooley, S., Kustka, A.B., Montoya, J.P., Sañudo-Wilhelmy, S.A., Shipe, R., Capone, D.G., 2008. Amazon River enhances diazotrophy and carbon sequestration in the tropical North Atlantic Ocean. Proc. Natl. Acad. Sci. 105, 10460–10465. https://doi.org/10.1073/pnas.0710279105.

Tyaquiçã, P., Veleda, D., Lefèvre, N., Araujo, M., Noriega, C., Caniaux, G., Servain, J., Silva, T., 2017. Amazon Plume salinity response to ocean teleconnections. Front. Mar. Sci. 4.

Wijffels, S.E., Schmitt, R.W., Bryden, H.L., Stigebrandt, A., 1992. Transport of freshwater by the oceans. J. Phys. Oceanogr. 22, 155–162. https://doi.org/10.1175/1520-0485(1992)022<0155:TOFBTO>2.0.CO;2.